Stacking defects in GaP nanowires: Electronic structure and optical properties

Divyanshu Gupta,[1] Nebile Isik Goktas,[2] (ID) Amit Rao,[2] Ray LaPierre,[2] (ID) and Oleg Rubel[1,a)] (ID)

AFFILIATIONS

[1]Department of Materials Science and Engineering, McMaster University, 1280 Main Street West, Hamilton, Ontario L8S 4L7, Canada
[2]Department of Engineering Physics, McMaster University, 1280 Main Street West, Hamilton, Ontario L8S 4L7, Canada

[a)]rubelo@mcmaster.ca

ABSTRACT

Formation of twin boundaries during the growth of semiconductor nanowires is very common. However, the effects of such planar defects on the electronic and optical properties of nanowires are not very well understood. Here, we use a combination of *ab initio* simulation and experimental techniques to study these effects. Twin boundaries in GaP are shown to act as an atomically narrow plane of wurtzite phase with a type-I homostructure band alignment. Twin boundaries and stacking faults (wider regions of the wurtzite phase) lead to the introduction of shallow trap states observed in photoluminescence studies. These defect states may cause undesired radiative or nonradiative recombination impacting on the performance of nanowire-based devices.

I. INTRODUCTION

III-V semiconductor nanowires (NWs) have applications in electronic, optoelectronic, and photonic devices.[1] III-V NWs can be grown epitaxially on Si making integration of III-V optoelectronic devices with Si-based technology possible.[2–4] NWs with embedded quantum dots (e.g., GaAs quantum dots in GaP NWs) have shown potential for use in light-emitting diodes (LEDs), lasers, and photodetectors.[5]

Crystal imperfections in $\langle 111 \rangle$ oriented III-V NWs are one of the factors that can limit the performance of optoelectronic devices. Twin boundaries (TBs) are one of the most abundant planar defects observed in NWs[6] as well as bulk semiconductors.[7] A very high twin plane density is usually observed in NWs due to their relatively low stacking fault energy,[8] especially for GaP (30 meV/atom),[9] which can be easily overcome at typical NW synthesis temperatures. Planar crystal defects, such as TBs and stacking faults, can affect electron transport by acting as a carrier scattering source,[10,11] a recombination center,[12–14] or a trap.[15,16] Unwanted radiative or nonradiative recombination associated with midgap states can be detrimental to the efficiency of optoelectronic devices such as removing carriers from the desired recombination channel in lasers or LEDs or reducing carrier collection in photovoltaic cells. Furthermore, studies have shown that it is possible to synthesize twinning superlattice structure with long-range order,[17] which

could allow for tuning of optical properties in NW devices. Understanding the potential effects of such defects on the electronic and optical properties of NWs is critical for NW optoelectronic devices.

Here, we present structural and optical studies of GaP NWs combined with *ab initio* calculations to establish a structure-property relationship. Despite GaP being an indirect semiconductor, photoluminescence (PL) spectra of GaP NWs show optical transitions at energies lower than the fundamental bandgap of bulk GaP. Transmission electron microscopy (TEM) analysis of NWs indicates that GaP is present in the zinc blende (ZB) phase along with the existence of TBs. We use density functional theory (DFT) to establish a model of the $\langle 111 \rangle$ TB in GaP and propose an effective band diagram that explains the origin of sub-bandgap optical transitions.

II. METHOD

A. Experimental details

GaP NWs were grown on (111) Si by the self-assisted (seeded by a Ga droplet) selective-area epitaxy method using a multisource (In,Ga,Al,As,P,Sb) molecular beam epitaxy system. A solid source effusion cell was used for Ga, while the group V source was P_2 obtained from a high temperature (950 °C) PH_3 cracker cell. NW
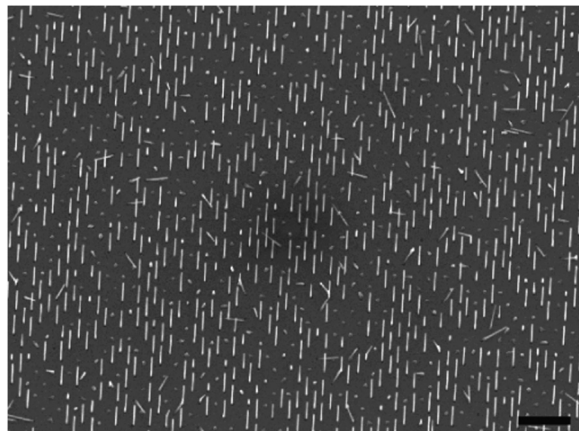
FIG. 1. 30° tilted view SEM image of GaP NWs. Scale bar is 1 μm.

growth took place with a Ga impingement rate of 0.125 μm/h, a V/III flux ratio of 2, and a substrate temperature of 600 °C. Details of the growth are presented elsewhere.[18] After growth, NW arrays were characterized by scanning electron microscopy (SEM) using a JEOL 7000F operating at 5 kV. The SEM image in Fig. 1 indicated NWs with ≈1 μm length.

The NW structure was investigated in a FEI Titan 80-300 LB aberration-corrected scanning transmission electron microscope (STEM) operating at 300 keV. The NWs were removed from their growth substrate for STEM investigation by sonication in a methanol solution followed by transfer to a holey carbon grid. NWs had 50 nm diameter as evident from the dark-field STEM image in Fig. 2(a). The Ga droplet used for the self-assisted NW growth is evident in the bottom-right of the STEM image. A high-resolution TEM (HRTEM) image in Fig. 2(b) and the Fourier transform of the image (inset) indicate a twinned ZB crystal structure with stacking faults (SFs), which is also evident by the contrast stripes in Fig. 2(a). Figure 2(c) shows the atomic stacking sequence along the [111]B growth direction of the NW, showing the ZB twins separated by the SFs.

Microphotoluminescence (μPL) measurements were performed at 10 K on individual NWs. Single NWs were prepared

by dispersion on an oxidized Si substrate. An Ar$^+$ laser with a wavelength of 488 nm was used for excitation through a 60× objective. Spectra were collected by a 0.55 m Horiba Jobin Yvon spectrometer and dispersed onto a LN$_2$ cooled Si CCD detector. The μPL spectra (Fig. 3) indicated sharp lines below the bandgap of bulk GaP.

B. Computational details

The first-principles calculations were carried out using DFT[19] and a projector augmented wave method implemented in the Vienna *ab initio* simulation package[20–22] (VASP). The lattice constant of GaP-ZB 2-atom primitive cell was optimized using self-consistent metageneralized gradient approximation (SCAN)[23] for the exchange and correlation functional. The cut-off energy for the plane-wave expansion was set at 340 eV, which is 25% higher than the value recommended in pseudopotentials. Ga_d and P pseudopotentials were used for structural optimizations. The structure was relaxed by minimizing Hellmann-Feynman forces below 2 meV/Å. To capture the localized wurtzite (WZ) region at a twin boundary in a ZB-GaP nanowire, the 4-atom primitive structure of WZ GaP was lattice matched to ZB along the a and b axis while relaxing stress along the c axis. The Brillouin zone of the primitive cells was sampled using $8 \times 8 \times 8$ and $8 \times 8 \times 5$ k meshes for ZB and WZ structures, respectively. The Heyd-Scuseria-Ernzerhof[24] screened hybrid functional (its HSE-06[25] version) was used in calculations of bandgaps and band alignments (VASP tags HFSCREEN = 0.2 and AEXX = 0.25). The Ga_d potential was substituted by Ga_vs_GW potential with 3s valence electrons in band alignment calculations when a Ga 3s reference state was used. The spin-orbit interaction was ignored. The calculated structural parameters and bandgaps for ZB and WZ phases of GaP are listed in Table I.

A supercell of ZB GaP was created along the [111] direction as shown in Fig. 4(a). Along the [111] direction the normal stacking sequence is . . . ABCABC . . .. Two 180° twin boundaries were created by altering the stacking sequence as shown in Fig. 4(b). The structures can be accessed at the Cambridge crystallographic data center (CCDC) under deposition numbers 1870794 and 1870797, respectively. The supercell relaxation was performed by minimizing Hellmann-Feynman forces below 2 meV/Å and stresses below
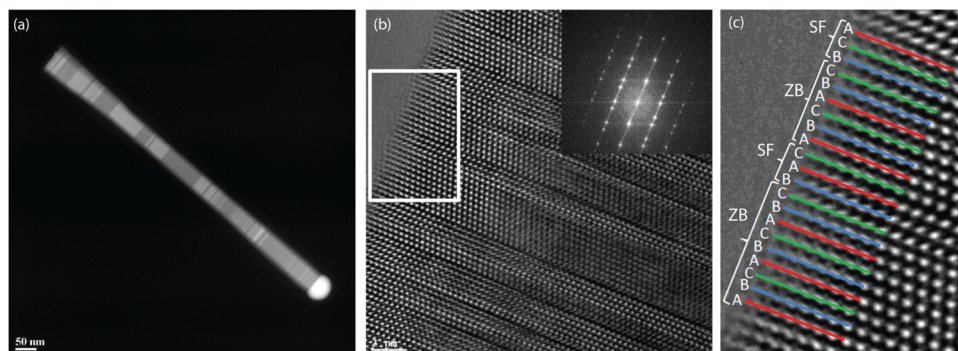

FIG. 2. (a) Dark-field STEM image of a single GaP NW. Scale bar is 50 nm. (b) HRTEM image near the sidewall of a single NW. Scale bar is 2 nm. Inset shows the Fourier transform of the image, indicating a twinned ZB crystal structure. (c) Magnified view of the white box in (b), showing the atomic stacking sequence with ZB segments separated by stacking faults (SFs).
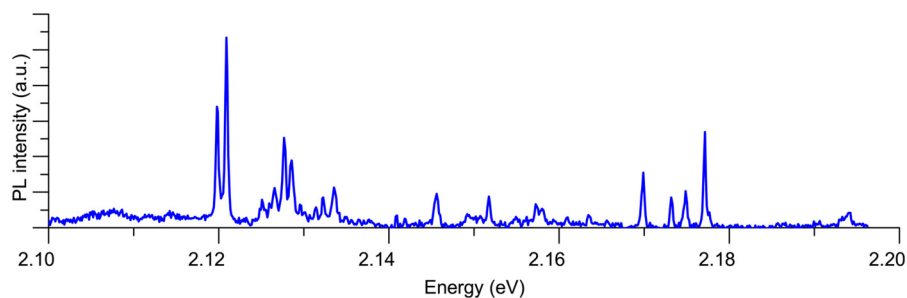
FIG. 3. Low temperature (10 K) μPL spectra obtained from a single GaP NW.

0.1 kbar using a $6 \times 6 \times 1$ k-mesh grid and the SCAN functional. Subsequently, electronic states were calculated with the HSE-06 functional using a $6 \times 6 \times 1$ k-mesh grid.

To present the band structure of the WZ phase in the f.c.c. Brillouin zone, a supercell was constructed based on a 4-atom WZ primitive cell by applying the following transformation (rotation) matrix in VESTA software,[26]

$$P = \begin{pmatrix} 1 & 0 & 2 \\ 0 & 1 & 2 \\ 0 & 0 & 3 \end{pmatrix}. \qquad (1)$$

An advantage of the resultant 12-atom supercell is its compatibility with f.c.c. translational lattice vectors (the multiplicity of $1 \times 1 \times 6$). The latter allows us to use a band structure unfolding[27] as implemented in the fold2Bloch utility[28] and present the WZ band structure in the same Brillouin zone as used for the ZB phase.

III. RESULTS AND DISCUSSION

Optical transitions with energies lower than the fundamental bandgap of 2.34 eV[29] for bulk GaP (at 10 K) observed in the PL spectrum (Fig. 3) indicate the presence of localized energy states within the bandgap, possibly arising due to TBs and SFs. To explore the spatial distribution of charge carriers, the plane averaged wave function amplitude $|\psi(r)|^2$ distribution in the supercell was calculated using HSE-06[25] exchange and correlation functional. According to wave function amplitude distributions along the c axis shown in Fig. 5(a), the defect-free structure displays a uniform

wave function amplitude distribution in the supercell, whereas for the structure with TBs [Fig. 5(b)], states at the conduction band edge (CBE) and valence band edge (VBE) are both accumulated at the TB. Furthermore, the degree of localization is more prominent for the CBE than for the VBE. Additionally, a structure was constructed to simulate the presence of an extended WZ segment at twin boundaries as illustrated in Fig. 5(c). The wave function amplitude for CBE and VBE is again spatially localized. The degree of localization is similar for CBE and VBE. It is also found that two envelope functions in Fig. 5(c) are asymmetric, indicating the presence of an electric field in the crystal along the c axis. First, we investigate the origin of localization of the electrons and holes at the defect regions.

To understand the origin of this localization, the atomic arrangement in the defected supercell was analyzed. Group III-V semiconductors adopt a ZB or WZ type atomic arrangement depending on ionicity of the bond. GaP, being relatively less ionic, naturally exhibits a ZB structure with WZ structure being unstable in bulk. However, in the NW configuration, the WZ structure can become progressively more favorable under certain growth conditions or as the NW diameter decreases.[30] Structures in Fig. 4 can be viewed as a sequence of bilayers (one group-III and one group-V atom per bilayer) stacked along the $\langle 111 \rangle$ direction. The ZB structure follows an ...ABCABC... stacking sequence of those bilayers as shown in Fig. 4(a), while the WZ phase exhibits an ...ABAB... sequence where each letter represents a bilayer of the III-V pair. A TB in the ZB phase can be regarded as a stacking fault, which creates a local atomically narrow plane of WZ phase[31] (pp. 55–57) as illustrated in Fig. 6. The coexistence of ZB/WZ segments within a structure has been referred to as polytypism. This effect has been studied for multiple systems including GaP,[32] GaAs,[33] InP,[34] InAs,[35] ZnO,[36] Si,[37] and other III-V and II-VI compounds and has been shown to have a significant impact on the optical and electronic properties of the materials. Assali et al.[32] have shown controlled growth of WZ/ZB GaP superstructures by modulating the vapor-liquid-solid growth parameters.

Electronic and optical properties of the WZ[38] phase are very different from its ZB counterpart. This difference could explain the unexpected PL transitions. Previous experimental and theoretical investigations suggest that the GaP-WZ structure is a pseudodirect band gap material with a lower bandgap of 2.13 eV (at 4 K) as compared to 2.34 eV (at 10 K) for the GaP-ZB structure.[39,40] To predict the effects of narrow WZ regions in the ZB phase, it is crucial to establish the relative alignment of CBE and VBE in the two phases.
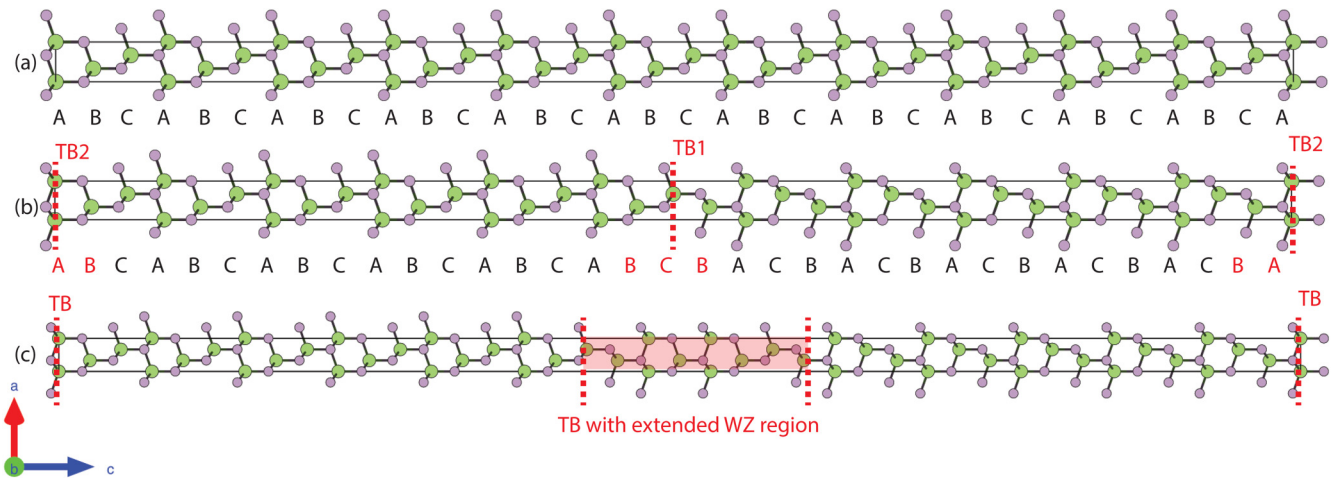
TABLE I. Calculated and experimental structural parameters (a and c) and bandgap (E_g) of GaP in two phases.

Phase	Parameter	Theory (VASP)	Experimental (at T)
ZB	a (Å)	5.449	5.446 (300 K)[56]
	E_g (eV)	2.30	2.34 (10 K)[29]
WZ on ZB	a (Å)	3.853[a]	3.842[57]
	c (Å)	6.339	6.335[57]
	E_g (eV)	2.15	2.13 (4 K)[58,59]

[a]The value is set at $a^{WZ} = a^{ZB}/\sqrt{2}$ to maintain the interface with ZB structure, while c^{WZ} is allowed to relax (CCDC No. 1870795).

FIG. 4. (a) 66-atom GaP-ZB supercell with atomic sequence ABCABC... along the [111] direction (*c* axis) without any defects (CCDC No. 1870794). (b) 68-atom GaP-ZB supercell with 2 twin boundaries TB1 and TB2 (CCDC No. 1870797). (c) 80-atom ZB GaP supercell with stacking fault consisting of an extended WZ region (CCDC No. 1870796).

Prior theoretical studies suggest that III-V semiconductors in a WZ/ZB homostructure generally follow a type-II band alignment.[41] This type of the band alignment will favor a spatial separation of electrons and holes at the WZ/ZB interface. In the case of GaP, literature shows a disagreement about the band alignment between the ZB and WZ phase. An early theoretical work by Murayama and Nakayama[41] proposed a type-II alignment, whereas later results by Belabbes *et al.*[14] claim a type-I alignment. Polarization-dependent PL measurement reported by Assali *et al.*[42] support a type-I alignment. It should be noted that Murayama and Nakayama[41] used a local density approximation for the exchange and correlation functional for calculation of band offsets leading to a significant underestimation of bandgaps for ZB as well as WZ phases. Furthermore, the WZ structures used for these calculations were completely relaxed, which would not be applicable to a homojunction because the WZ present at the TB would be lattice matched to the ZB phase along the *a* and *b* axis leading to an epitaxial strain in the *a-b* plane, while the relaxation of stress along the *c* axis is permitted. This necessitates a further investigation into the band alignment pertaining to the present case.

An average Coulomb potential serves as a reference energy in DFT calculations of solids with periodic boundary conditions. This reference energy is ill-defined due to the lack of vacuum. Thus, band alignments cannot be derived directly from eigenvalues of ZB and WZ structures obtained from separate calculations. The first step to reliably determine the relative position of band edges in the two phases is to identify a reference state that does not change with the crystal structure. Core states are an ideal candidate for this purpose as these states are least sensitive to local coordination of atoms and thus should be virtually unaffected by changes in the valence electron density (see the Appendix for a rigorous evaluation of the associated inaccuracy). This approach was successfully applied to the calculation of volume deformation potentials in

III-V and II-VI semiconductors.[43] Eigenvalues of the 3*s* state of Ga are obtained for bulk ZB and WZ structures from separate calculations (WZ is lattice matched to ZB along the *a* and *b* axis and allowed to relax along the *c* axis). Figure 7(a) shows a qualitative representation of the alignment of eigenvalues in ZB and WZ structures. Note that Ga 3*s* states are slightly misaligned due to uncertainties in the reference energy between the two calculations. The difference in the 3*s* state of Ga is adjusted by shifting the WZ bands by

$$\Delta E_{3s} = E_{3s}^{Ga,WZ} - E_{3s}^{Ga,ZB}. \tag{2}$$

The adjusted band alignment is displayed in Fig. 7(b). The discontinuity in the valence band (ΔE_{VBE}) and that in the conduction band (ΔE_{CBE}) are evaluated as

$$\Delta E_{VBE/CBE} \approx E_{VBE/CBE}^{WZ} - E_{VBE/CBE}^{ZB} - \Delta E_{3s}. \tag{3}$$

Calculations using HSE-06 exchange-correlation functional yield $\Delta E_{VBE} = 137$ meV and $\Delta E_{CBE} = -20$ meV. In comparison, Belabbes *et al.*[14] obtained $\Delta E_{VBE} = 135$ meV and $\Delta E_{CBE} = -14$ meV with a completely relaxed WZ structure. The approximate sign in Eq. (3) indicates a small inaccuracy of ∼5 meV in the ΔE_{3s} term associated with a shift of E_{3s}^{Ga} energies at the WZ/ZB interface (see the Appendix for details).

Calculations with HSE-06 functional indicate a type-I band alignment for the WZ/ZB GaP homojunction, which agrees with the spatial localization of CBE and VBE states in Fig. 5. However, a stronger spatial localization of the CBE state in Fig. 5 suggests their stronger quantum confinement, which seems contradictory to the band alignment results. It should be noted that the alignment calculations are done for the band edges without paying attention to
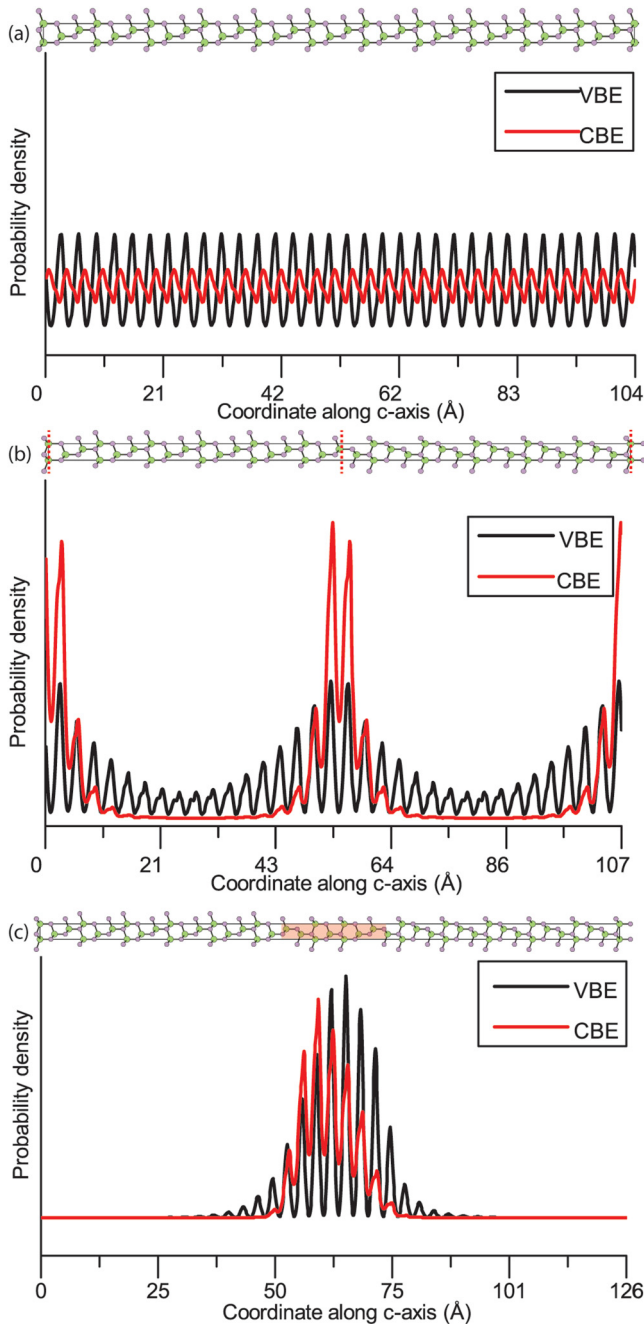
FIG. 6. Twin boundary (TB) in ZB resulting in a narrow WZ phase.

band edges belong to different points in the f.c.c. Brillouin zone (Δ_1 vs Λ_1 for the CBE) as shown in Fig. 8. Alternatively, the band alignment in the conduction band can be evaluated at the same Λ_1 point for both structures, resulting in a much deeper confinement potential for electrons. A similar situation takes place in GaAs/AlAs quantum wells, where it is customary to consider an electron localized in a GaAs domain as confined by a potential barrier corresponding to the energy difference between Γ_{1c} states of AlAs and GaAs.[44]

The accuracy of band alignment is further validated by using a more traditional and well established method laid down by Van de Walle and Martin,[45] which involves examining the macroscopic average of the electrostatic potential determined in the bulklike regions of each phase in a supercell (further details can be found in the Appendix). The two methods showed values of the band discontinuity within 10 meV of one another.

The calculated band offsets can now be used to assess a quantization energy. In GaP-WZ/ZB homostructures, the trap states are relatively shallow [Fig. 9(a)] due to the narrow width of TBs and the associated quantization of the electron and hole states. The energy of recombination of excitations trapped at TBs can be

FIG. 5. Planar average of DFT-HSE orbitals along the c axis for VBE and CBE in (a) defect-free structure, (b) structure with twin defects, and (c) structure with the extended WZ region.

the band character. In ordinary heterostructures, e.g., (InGa)As/GaAs, band edges of the quantum well and the barrier material are both located in the same k point of the Brillouin zone. However, this is not the case in the WZ/ZB GaP homostructure where the
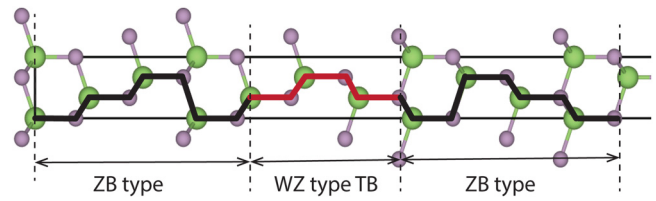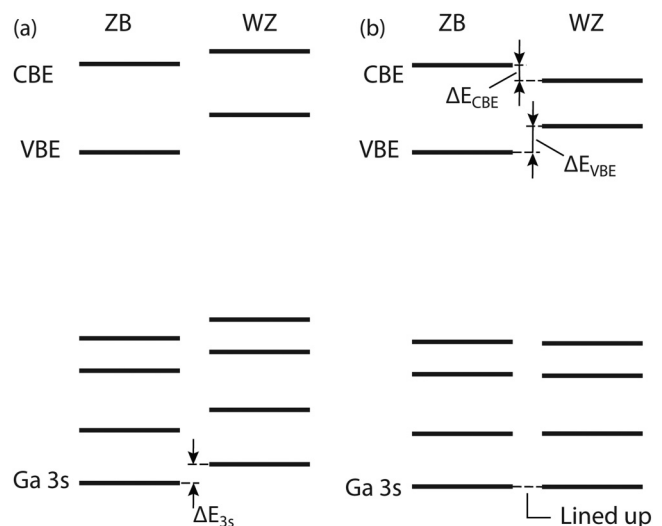

FIG. 7. Relative arrangement of energy levels in the ZB and WZ GaP primitive unit cell (a) prior to band alignment and (b) after the alignment of Ga 3s states.
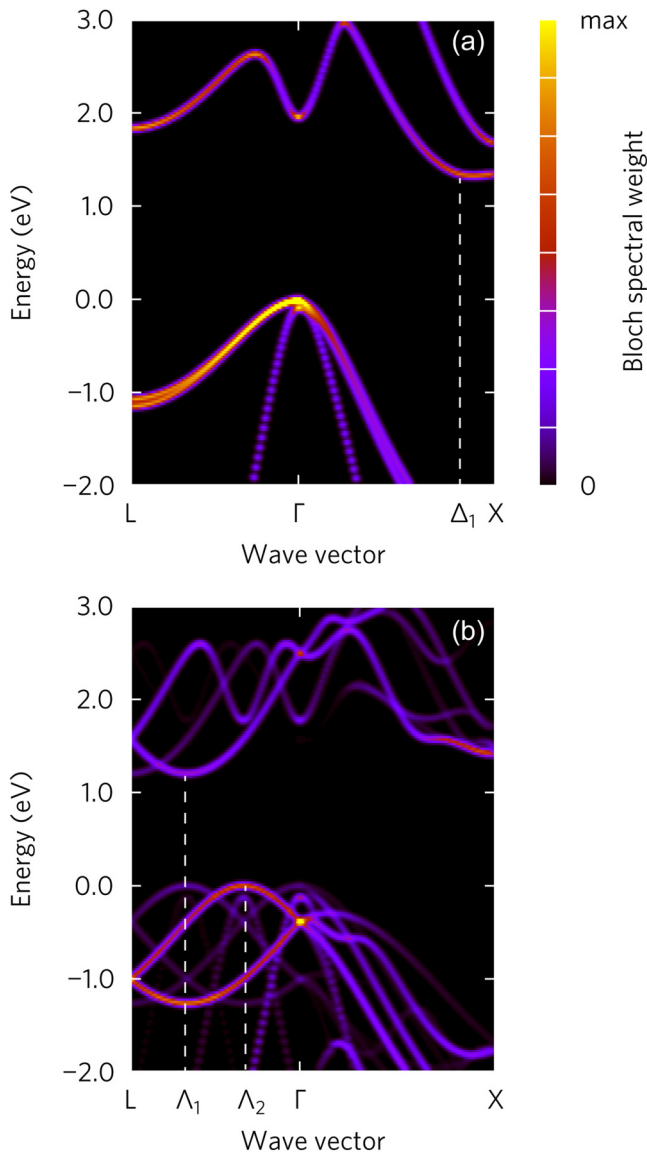
FIG. 8. Band structure of GaP in the (a) ZB phase and the (b) WZ phase presented in the f.c.c. Brillouin zone. Band edges of the two structures are at different k points. The WZ phase also shows an indirect bandgap, which explains why its lowest energy transition is dipole-forbidden,[39] even though the band structure appears direct when presented in the hexagonal Brillouin zone (both band edges fall into the Γ point). Calculations were performed with the PBEsol[54] exchange correlation functional. An origin of the energy scale is set at the Fermi energy.

FIG. 9. Quantization of energy levels in (a) narrow and (b) wide WZ regions embedded in the ZB phase.

calculated using a solution of the Schrödinger wave equation for a one-dimensional finite potential well as follows:[46]

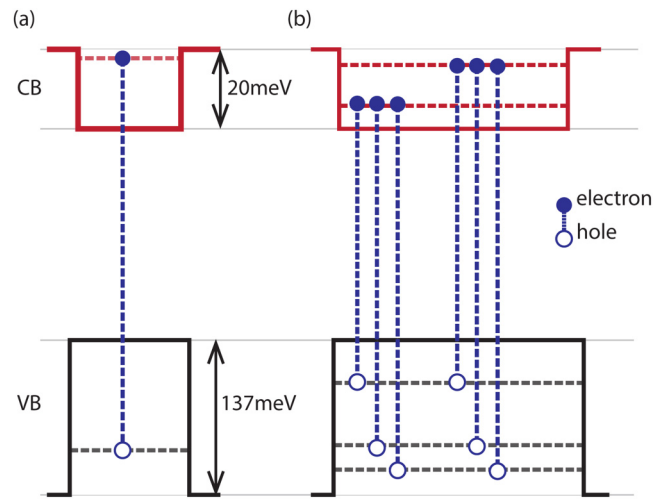$$\tan\left(\frac{L\sqrt{2mE}}{2\hbar}\right) = \sqrt{\frac{V-E}{E}}, \tag{4}$$

where $\hbar$ is the reduced Plank's constant, m is the effective mass of the hole (electron), V is the depth of potential well, i.e., ΔE_{VBE} or ΔE_{CBE}, E is the quantized energy level within the well, and L is the width of the well. The effective mass of electrons is taken as $1.12m_e$[47] (p. 104) and the effective mass of holes (heavy hole) is taken as $0.79m_e$[47] (p. 104), where m_e is the rest mass of the electron. The recombination energies are obtained for varying potential well widths starting at 2 WZ monolayers (MLs) ($L = 6.32\,\text{Å}$), i.e., a twin boundary, and widening with 2 ML intervals to simulate regions with extended WZ segments. Transition energies were calculated to a width of 8 MLs beyond which the difference in energy levels was less than 1 meV. Qualitatively, we see a higher number of states within the well along with progressively lower recombination energies as the potential well widens [Fig. 9(b)]. The transition energies thus obtained are plotted against the experimental μPL spectrum in Fig. 10. A Gaussian broadening with a full width at half maximum of 1 meV has been assigned to the calculated transition energies. The calculated spectrum was red-shifted by 35 meV to account for a minor inaccuracy in the bandgap calculated by HSE-06. The substructure for peaks lying in a width of 5 meV was found to be too narrow for splitting due light/heavy hole mass. Similar substructure has been observed by Koteles *et al.*[48] in case of GaAs where it has been shown to arise from excitons bound to impurities. The transition arising from an isolated twin boundary is expected near 2.22 eV. No transition peak above the energy of 2.2 eV is observed, because lower energy transitions created by quantum wells from the stacking defects are favored. We consider only heavy holes for our calculation as transition energies arising from light holes [effective mass $0.14m_e$[47] (p. 104)]. The transition energies calculated using a simple finite potential well model are in agreement with the experimental data (Fig. 10).
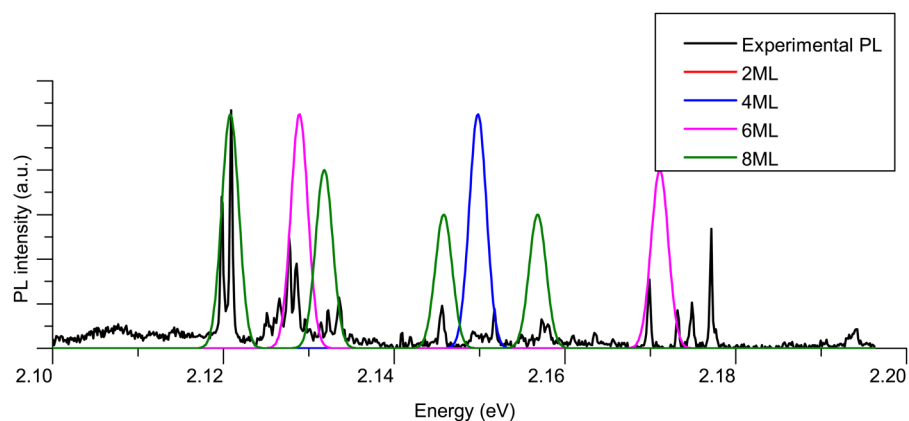
FIG. 10. Comparison of the experimental μPL spectrum and calculated electronic transition in the WZ/ZB GaP quantum wells of variable width [Fig. 9(b)].

Finally, we discuss the asymmetric nature of the probability density distribution seen in Fig. 5(c). Group III-V WZ structures exhibit a spontaneous polarization along the (0001) axis,[49] resulting in a built-in electric field in ZB and WZ segments that causes a charge segregation at the WZ/ZB interface. This effect has been widely studied[49–51] in various III-V compounds. It has also been shown that change in absolute as well as relative thickness of ZB and WZ phases lead to variation in the intensity of the built-in electric field. Wider WZ segments result in a stronger electric field and, hence, more prominent charge segregation.[52] Similar behavior is expected for GaP. This segregation is expected to be present at a twin boundary as well as adjacent SFs acting as wide WZ regions with a higher electric field as compared to an isolated twin boundary, which leads to a stronger segregation of charge carriers seen in Fig. 5(c).

IV. CONCLUSION

The effect of twin boundaries and stacking faults on electrical and optical properties of GaP nanowires was studied using experimental techniques in combination with *ab initio* density functional simulations. Transmission electron microscopy examination of GaP nanowires shows the presence of a zinc blende phase with twin boundaries and extended WZ segments. Photoluminescence studies of the nanowires show the presence of radiative recombination below the fundamental bandgap of zinc blende GaP. Twin boundaries can be viewed as an atomically narrow wurtzite phase. *Ab initio* calculations suggest that the WZ/ZB GaP homostructure shows a type-I band alignment. Thus, the twin boundary acts as shallow trap for electrons and holes. The energy of recombination of excitations trapped at twin boundaries is expected to be approximately 60 meV below the fundamental bandgap of zinc blende GaP. Photoluminescence lines with lower energies can arise from stacking faults (a few monolayers of the extended wurtzite region) at the twin boundaries.

APPENDIX: VALIDATION OF BAND ALIGNMENT CALCULATIONS

1. Average electrostatic potential

Band alignment determination using an averaged electrostatic potential was carried out according to the procedure outlined by Weston *et al.*[53] as an alternative to the alignment of Ga 3s core states used in the main part of the paper. Calculations were
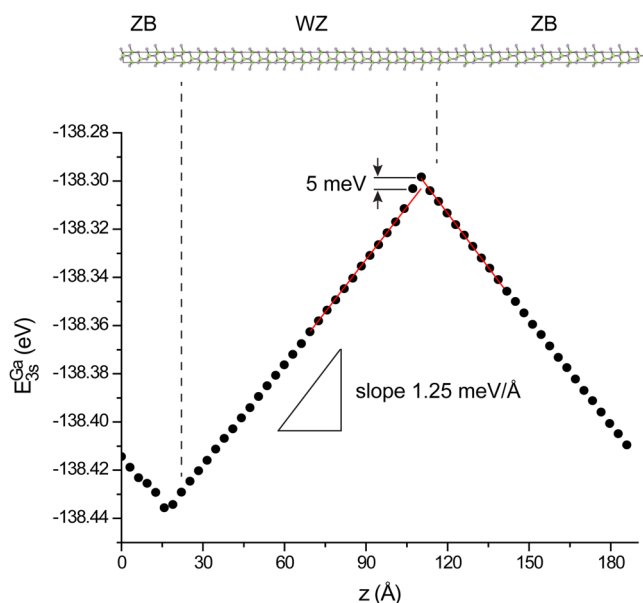

FIG. 11. Variation of Ga 3s core energy levels along the *c* axis in a 1:1 ZB:WZ GaP homostructure (top panel) composed of 120 atoms.

performed with VASP package employing PBEsol[54] exchange and correlation functional. First, the position of the valence band maxima is calculated with respect to the average electrostatic potential $\langle V \rangle_{\mathrm{B}}^{\mathrm{ZB(WZ)}}$ for both ZB and WZ structures in bulk. Furthermore, the average electrostatic potential $\langle V \rangle_{\mathrm{H}}^{\mathrm{ZB(WZ)}}$ is determined for bulklike ZB and WZ regions within a 1:1 ZB:WZ homostructure supercell with 120 atoms (not relaxed) shown in the upper panel of Fig. 11. The relative misalignment of the electrostatic potential is expressed as

$$\Delta V = \langle V \rangle_{\mathrm{B}}^{\mathrm{WZ}} - \langle V \rangle_{\mathrm{B}}^{\mathrm{ZB}} - \langle V \rangle_{\mathrm{H}}^{\mathrm{WZ}} + \langle V \rangle_{\mathrm{H}}^{\mathrm{ZB}}. \tag{A1}$$

Finally, the valence band offset ΔE_{VBE} is defined as

$$\Delta E_{\mathrm{VBE}} = E_{\mathrm{VBE}}^{\mathrm{WZ}} - E_{\mathrm{VBE}}^{\mathrm{ZB}} - \Delta V. \tag{A2}$$

The calculated band offset $\Delta E_{\mathrm{VBE}} = 110$ meV agrees with the corresponding value of 118 meV determined with PBEsol using Ga 3s core states as the reference [Eq. (3)]. Since both methods yield the same results, we prefer using the core states as a reference due to its simplicity.

2. Misalignment of core states

When Ga 3s core states are used as a reference for determining the band alignment, it is assumed that the E_{3s}^{Ga} energy in GaP is not sensitive to the crystal structure (ZB vs WZ). Accuracy of this approximation can be further tested by analyzing a discontinuity of E_{3s}^{Ga} at the WZ/ZB interface of the 120 atoms supercell discussed in the previous paragraph. The calculations were performed with the WIEN2k,[55] an all electron density functional package. The WIEN2k basis set is better suited than VASP for this purpose, since core states are confined within muffin tin spheres centered at individual atoms allowing for an easy link between E_{3s}^{Ga} values and atomic coordinates. The radii (R^{MT}) of the muffin tin spheres are chosen to be equal to 2.36 and 1.93 Bohr for Ga and P, respectively. The product of the minimum radius and the maximum cut-off wave vector in the reciprocal space was set at the value of $R_{\mathrm{min}}^{\mathrm{MT}} K_{\mathrm{max}} = 7$. The Brillouin zone was sampled using an $8 \times 8 \times 1$ k-point mesh. Evolution of E_{3s}^{Ga} core energy levels along the c axis of the supercell is shown in Fig. 11. A discontinuity in the E_{3s}^{Ga} energy level at the ZB/WZ interface is about 5 meV, which sets the error bar for band offsets obtained with this method.

The slope of energy levels in Fig. 11 indicates the presence of an electric field of equal magnitude 1.25 meV/Å, but opposite direction, in both WZ and ZB regions of the model. The field originates likely due to a spontaneous polarization present in the WZ structure. The effect becomes less notable in structures with narrow WZ regions as discussed at the end of Sec. III.

REFERENCES

[1]H. J. Joyce, Q. Gao, H. Hoe Tan, C. Jagadish, Y. Kim, J. Zou, L. M. Smith, H. E. Jackson, J. M. Yarrison-Rice, P. Parkinson, and M. B. Johnston, Prog. Quantum Electron. **35**, 23 (2011).

[2]Z. Zhou, B. Yin, and J. Michel, Light Sci. Appl. **4**, e358 (2015).

[3]T. Martensson, C. P. T. Svensson, B. A. Wacaser, M. W. Larsson, W. Seifert, K. Deppert, A. Gustafsson, L. R. Wallenberg, and L. Samuelson, Nano Lett. **4**, 1987 (2004).

[4]D. M. Geum, M. S. Park, J. Y. Lim, H. D. Yang, J. D. Song, C. Z. Kim, E. Yoon, S. H. Kim, and W. J. Choi, Sci. Rep. **6**, 20610 (2016).

[5]P. Kuyanov, S. A. McNamee, and R. R. LaPierre, Nanotechnology **29**, 124003 (2018).

[6]J. Johansson, L. S. Karlsson, C. P. T. Svensson, T. Mrtensson, B. A. Wacaser, K. Deppert, L. Samuelson, and W. Seifert, Nat. Mater. **5**, 574 (2006).

[7]D. T. Hurle, J. Cryst. Growth **147**, 239 (1995).

[8]R. E. Algra, M. A. Verheijen, L.-F. Feiner, G. G. W. Immink, R. Theissmann, W. J. P. V. Enckevort, E. Vlieg, and E. P. A. M. Bakkers, Nano Lett. **10**, 2349 (2010).

[9]H. Gottschalk, G. Patzer, and H. Alexander, Phys. Status Solidi A **45**, 207 (1978).

[10]X. Qian, M. Kawai, H. Goto, and J. Li, Comput. Mater. Sci. **108**, 258 (2015).

[11]K. Shimamura, Z. Yuan, F. Shimojo, and A. Nakano, Appl. Phys. Lett. **103**, 022105 (2013).

[12]M. Heiss, S. Conesa-Boj, J. Ren, H.-H. Tseng, A. Gali, A. Rudolph, E. Uccelli, F. Peiró, J. R. Morante, D. Schuh, E. Reiger, E. Kaxiras, J. Arbiol, and A. Fontcuberta i Morral, Phys. Rev. B **83**, 045303 (2011).

[13]N. Vainorius, D. Jacobsson, S. Lehmann, A. Gustafsson, K. A. Dick, L. Samuelson, and M.-E. Pistol, Phys. Rev. B **89**, 165423 (2014).

[14]A. Belabbes, C. Panse, J. Furthmüller, and F. Bechstedt, Phys. Rev. B **86**, 075208 (2012).

[15]K. Pemasiri, M. Montazeri, R. Gass, L. M. Smith, H. E. Jackson, J. Yarrison-rice, S. Paiman, Q. Gao, H. H. Tan, C. Jagadish, X. Zhang, and J. Zou, Nano Lett. **9**, 648 (2009).

[16]J. Wallentin, M. Ek, L. R. Wallenberg, L. Samuelson, and M. T. Borgstro, Nano Lett. **12**, 151 (2012).

[17]R. E. Algra, M. A. Verheijen, L.-F. Feiner, G. G. W. Immink, W. J. P. V. Enckevort, E. Vlieg, and E. P. A. M. Bakkers, Nano Lett. **11**, 1259 (2011).

[18]P. Kuyanov, J. Boulanger, and R. R. LaPierre, J. Cryst. Growth **462**, 29 (2017).

[19]W. Kohn and L. J. Sham, Phys. Rev. **140**, A1133 (1965).

[20]G. Kresse and D. Joubert, Phys. Rev. B **59**, 1758 (1999).

[21]P. E. Blöchl, Phys. Rev. B **50**, 17953 (1994).

[22]G. Kresse and J. Furthmüller, Phys. Rev. B **54**, 11169 (1996).

[23]J. Sun, M. Marsman, G. I. Csonka, A. Ruzsinszky, P. Hao, Y.-S. Kim, G. Kresse, and J. P. Perdew, Phys. Rev. B **84**, 035117 (2011).

[24]J. Heyd, G. E. Scuseria, and M. Ernzerhof, J. Chem. Phys. **118**, 8207 (2003).

[25]A. V. Krukau, O. A. Vydrov, A. F. Izmaylov, and G. E. Scuseria, J. Chem. Phys. **125**, 224106 (2006).

[26]K. Momma and F. Izumi, J. Appl. Crystallogr. **44**, 1272 (2011).

[27]V. Popescu and A. Zunger, Phys. Rev. Lett. **104**, 236403 (2010).

[28]O. Rubel, A. Bokhanchuk, S. J. Ahmed, and E. Assmann, Phys. Rev. B **90**, 115202 (2014).

[29]M. R. Lorenz, G. D. Pettit, and R. C. Taylor, Phys. Rev. **171**, 876 (1968).

[30]H. J. Joyce, J. Wong-Leung, Q. Gao, H. Hoe Tan, and C. Jagadish, Nano Lett. **10**, 908 (2010).

[31]J. Li, D. Wang, and R. R. LaPierre, *Advances in III-V Semiconductor Nanowires and Nanodevices* (Bentham Science Publishers, 2011), pp. 55–57.

[32]S. Assali, L. Gagliano, D. S. Oliveira, M. A. Verheijen, S. R. Plissard, L. F. Feiner, and E. P. A. M. Bakkers, Nano Lett. **15**, 8062 (2015).

[33]L. Ahtapodov, M. Munshi, J. S Nilsen, J. F Reinertsen, D. Dheeraj, B.-O. Fimland, A. Helvoort, and H. Weman, Nanotechnology **27**, 445711 (2016).

[34]F. Wang, C. Wang, Y. Wang, M. Zhang, Z. Han, S. Yip, L. Shen, N. Han, E. Y. B. Pun, and J. C. Ho, Sci. Rep. **6**, 32910 (2016).

[35]P. Caroff, K. A. Dick, J. Johansson, M. E. Messing, K. Deppert, and L. Samuelson, Nat. Nanotechnol. **4**, 50 (2008).

[36]A. B. Aebersold, L. Fanni, A. Hessler-Wyser, S. Nicolay, C. Ballif, C. Hébert, and D. T. Alexander, Acta Mater. **130**, 240 (2017).

[37]X. Liu, L. Liu, X. Wu, and P. K. Chu, Phys. Lett. A **379**, 1384 (2015).

[38]S. Assali, J. Greil, I. Zardo, A. Belabbes, M. W. A. de Moor, S. Koelling, P. M. Koenraad, F. Bechstedt, E. P. A. M. Bakkers, and J. E. M. Haverkort, J. Appl. Phys. **120**, 044304 (2016).

[39]A. Belabbes and F. Bechstedt, Phys. Status Solidi B **256**, 1800238 (2019).

[40]S. Assali, I. Zardo, S. Plissard, D. Kriegner, M. A. Verheijen, G. Bauer, A. Meijerink, A. Belabbes, F. Bechstedt, J. E. Haverkort, and E. P. Bakkers, Nano Lett. **13**, 1559 (2013).

[41]M. Murayama and T. Nakayama, Phys. Rev. B **49**, 4710 (1994).

[42]S. Assali, J. Lähnemann, T. T. T. Vu, K. D. Jöns, L. Gagliano, M. A. Verheijen, N. Akopian, E. P. A. M. Bakkers, and J. E. M. Haverkort, Nano Lett. **17**, 6062 (2017).

[43]S. H. Wei and A. Zunger, Phys. Rev. B **60**, 5404 (1999).

[44]A. Franceschetti and A. Zunger, Phys. Rev. B **52**, 14664 (1995).

[45]C. G. Van de Walle and R. M. Martin, Phys. Rev. B **35**, 8154 (1987).

[46]D. L. Aronstein and C. R. Stroud, Am. J. Phys. **68**, 943 (2000).

[47]M. E. Levinshteĭn, S. L. Rumyantsev, and M. Shur, *Handbook Series on Semiconductor Parameters, Vol. 1: Si, Ge, C (Diamond), GaAs, GaP, GaSb, InAs, InP, InSb*, Handbook Series on Semiconductor Parameters (World Scientific Publishing Company, 1996), p. 104.

[48]E. S. Koteles, J. Lee, J. P. Salerno, and M. O. Vassell, Phys. Rev. Lett. **55**, 867 (1985).

[49]F. Bernardini, V. Fiorentini, and D. Vanderbilt, Phys. Rev. B **56**, R10024 (1997).

[50]J.-M. Wagner and F. Bechstedt, Phys. Rev. B **66**, 115202 (2002).

[51]S.-H. Park, Superlatt. Microstruct. **120**, 611 (2018).

[52]K. Zhang, Y. Dai, Z. Zhou, S. U. Jan, L. Guo, and J. R. Gong, Nano Energy **41**, 101 (2017).

[53]L. Weston, H. Tailor, K. Krishnaswamy, L. Bjaalie, and C. G. Van de Walle, Comput. Mater. Sci. **151**, 174 (2018).

[54]J. P. Perdew, A. Ruzsinszky, G. I. Csonka, O. A. Vydrov, G. E. Scuseria, L. A. Constantin, X. Zhou, and K. Burke, Phys. Rev. Lett. **100**, 136406 (2008).

[55]P. Blaha, K. Schwarz, G. K. H. Madsen, D. Kvasnicka, J. Luitz, R. Laskowski, F. Tran, and L. D. Marks, *WIEN2K: An Augmented Plane Wave Plus Local Orbitals Program for Calculating Crystal Properties* (Techn. Universität Wien, Austria, 2018).

[56]R. E. Treece, G. S. Macala, and R. B. Kaner, Chem. Mater. **4**, 9 (1992).

[57]D. Kriegner, S. Assali, A. Belabbes, T. Etzelstorfer, V. Holý, T. Schülli, F. Bechstedt, E. P. A. M. Bakkers, G. Bauer, and J. Stangl, Phys. Rev. B **88**, 115315 (2013).

[58]N. N. Halder, S. Cohen, D. Gershoni, and D. Ritter, Appl. Phys. Lett **112**, 133107 (2018).

[59]J. Greil, S. Assali, Y. Isono, A. Belabbes, F. Bechstedt, F. O. Valega Mackenzie, A. Y. Silov, E. P. A. M. Bakkers, and J. E. M. Haverkort, Nano Lett. **16**, 3703 (2016).